ELSEVIER

International Journal of Solids and Structures 41 (2004) 5929–5943

INTERNATIONAL JOURNAL OF SOLIDS and STRUCTURES

www.elsevier.com/locate/ijsolstr

An experimental and numerical study of the compaction of alumina agglomerates

Y.Y. Foo *, Y. Sheng, B.J. Briscoe

Department of Chemical Engineering and Chemical Technology, Imperial College London, Prince Consort Road, London SW7 2AZ, UK

Received 23 April 2004
Available online 3 July 2004

Abstract

A series of experimental uniaxial single-ended compaction tests and associated numerical simulations based upon the discrete element (DE) and finite element (FE) methods are described. The numerical results show a good correlation with the experimental results. Both of the results, experimental and numerical, indicate that a complete compaction process consists of at least three types of distinct stages; namely particle rearrangement; deformation and breakdown of the agglomerates; and strain hardening of the green compact. The average coordination number of the particle increases as the densification of the bulk assembly progresses. The evolution of the inhomogeneity of the internal structure of a green body, which is primarily caused by the frictional work between the die wall and the adjacent particles, was investigated. The numerical results show that the highest density regions form at the top circumference of the green compact whereas the bottom circumference has the lowest density region.

Keywords: Agglomerates; Compaction; Inhomogeneity; Finite element; Discrete element

1. Introduction

Uniaxial die-pressing of ceramic powders is commonly adopted in order to produce "green" ceramic components with a desirable geometrical shape. A "green" compact is a term given to describe the product of the compression process prior to subsequent sintering or the application of the other finishing processes. The compaction method has exceptional merits in terms of the simplicity and speed of its operation. From the economical point of view, it does not involve relatively expensive machining and heavy manpower. A major drawback of this method is the formation of the internal structure gradient (Briscoe and Sinha, 1997; Cooper and Goodnow, 1962; Train, 1957) caused by the wall frictional work exerted during the compression process. A desirable coherent compressed green compact is essential to meet a certain mechanical strength criterion in order to withstand the post-compaction handling, such as packaging and storage.

* Corresponding author. Tel.: + 44-7717846466; fax: +44-2078522001.
E-mail address: yoong.foo@imperial.ac.uk (Y.Y. Foo).

0020-7683/$ - see front matter © 2004 Elsevier Ltd. All rights reserved.
doi:10.1016/j.ijsolstr.2004.05.053

Capping and lamination (Train, 1957) are classified as the most severe defects that may occur if the internal structural inhomogeneity is extensive. Capping refers to the nature of a compact at which the top part of the compact tends to detach easily from the green body. Lamination relates to the internal cracking of a green compact that weakens the green body strength. Moreover, warping or shape distortion due to the inhomogeneous shrinkage of the green compacts may occur during the subsequent sintering process. Therefore, the final sintered product may not be the required geometric replica which has the anticipated shape and dimension. Additional machining and grinding, which are normally slow, inefficient and costly, are then required to provide the required external structure and shape of the sintered products. The desire for near-net-shape forming (Aydin, 1994; Aydin et al., 1996; Ozkan, 1994) of the green compacts is therefore particularly important in the manufacturing of ceramic components.

This paper describes a study that aims to provide a better understanding about the compaction mechanisms and the evolution of the structural non-uniformity within an alumina green compact. Pressure–volume interrelationships were obtained from the experimental data of the uniaxial single-ended compacts, die-pressed at various ultimate compression pressures, in order to interpret the various compaction stages. The compaction processes were numerically simulated using the discrete element method (DEM) in order to rationalise the experimental results. In addition, the finite element method (FEM) was also used to study the evolution of the structural inhomogeneity within these green compacts. Internal low and high local density regions of a green compact were quantified. The physical morphologies of the mentioned regions were identified by examining the cross-sectional visualised images of the green compacts using scanning electron microscopy (SEM).

2. Experimental techniques

2.1. Preparation of alumina agglomerates

When the van der Waals forces between fine powders are dominant over the inertial forces of the bulk assembly, fine powders tend to aggregate simultaneously during their flowing process, eventually giving rise to many practical flowability problems. Consequently, fine powders are commonly agglomerated to increase the net size in order to facilitate their flow properties as well as lowering the potential industrial risks associated with their processing. Some of the most common agglomeration or granulation methods include tumbling, mixing, dispersion, thermal, drum and spray-dried methods. Binders are commonly added as processing aids in the agglomeration process in order to bind the particles together. The size, strength and properties of the agglomerates depend upon the quantity and quality of the binders applied. In turn, the use of binder affects the compact behaviour. The green density of compacts consisting of agglomerates and higher binder amounts is larger than that for the agglomerates containing lower binder amounts under the same compaction conditions (Ozkan, 1994).

The ceramic powders used in this study were commercial alumina (Al_2O_3) powders (Grade AESO-11C, MinChem Ltd, UK) of 0.4 μm mean particle size. The fine powders were granulated batchwise by means of the drum granulation method. An aqueous solution of a polymeric binder, poly (vinylalcohol) (PVA) (Harco 72.5, Harco Ltd, UK), was sprayed to the fine powders in a rotating drum in order to obtain agglomerates of reproducible size and shape. The alumina agglomerates were then sieved using conventional mesh sieves (Endecotts, UK) of standard size apertures 75, 150, 250, 425 and 600 μm in order to classify the agglomerate size; the scanning electron microscopic images of the alumina agglomerates used are shown in Fig. 1. Although the agglomerates were irregular in shape, they were assumed to be spherical for subsequent numerical analysis. In this study, ca. $\geqslant 425$ μm diameter agglomerates were used.

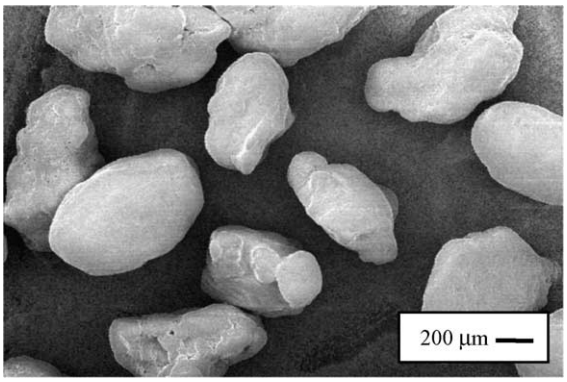

Fig. 1. Images of agglomerated alumina powders taken by scanning electron microscopy.

2.2. Uniaxial single-ended die-pressed compaction

A universal testing machine (EZ 50, Lloyds Instrument Ltd., UK), which consisted of a 50 kN maximum load cell transducer, was used to compress the alumina agglomerates. The schematic diagram of the universal testing machine is presented in Fig. 2. The alumina agglomerates were initially poured into a square (12 mm × 12 mm × 7 mm) stainless-steel rigid die. No special filling method was adopted. The movable top punch was made to descend in order to compress the alumina agglomerates until the desirable compaction pressure, i.e. 100 MPa was reached. The displacement–force data were collected and transferred to a computer. To allow the ejection of the green compact from the die, the static bottom punch in the die was removed.

The above-mentioned procedures were also repeated using a cylindrical stainless-steel die (Specac Ltd., UK), which had an internal diameter of 20 mm, to produce cylindrical compacts that were die-pressed at ultimate pressures of 20 and 100 MPa. Diametrical compressive rupture tests, Brazillian tests, were

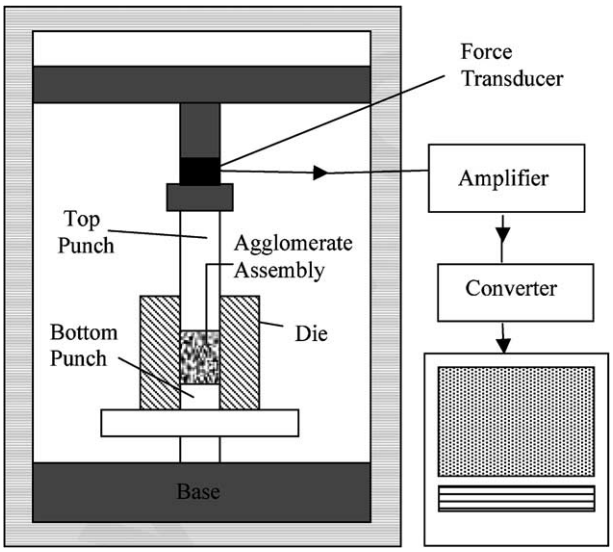

Fig. 2. Schematic representation of a uniaxial testing machine.

implemented in order to section the cylindrical green compacts into two symmetrical parts. The cross-sections of the green compacts were gold-coated and, subsequently, scanned by the scanning electron microscope (SEM) to obtain the images for morphological analysis and classification of the internal regions.

3. Numerical simulations

3.1. Discrete element method

The discrete element method (DEM), which was initially developed for applications with granular materials (Cundall and Strack, 1979), is an effective numerical tool to investigate the micro mechanics of granular materials. In the DEM, each individual particle of an assembly is modelled separately and its motion is defined from the interactions with neighbouring particles (Oda and Iwashita, 1999). The detailed movements of particles can be traced. As a consequence, microscopic evolution of the internal stress and the structure of the assembly can be obtained. The macro behaviour of the whole assembly can then be obtained by statistical means. In this study, a 3-D DEM code TRUBAL (Thornton and Yin, 1991; Thornton and Sun, 1993) is used to simulate the quasi-static uniaxial compaction of alumina agglomerates. The TRUBAL code is a powerful model used to simulate the deformations of spherical particles. The particles in this case refer to the alumina agglomerates. This modified model is generally based on elastic Hertzian type contacts but incorporation of 'overlapping' contacts in the simulations may tolerate some effective plastic contact deformations. Since the experimental compaction tests most certainly comprise a significant fraction of elastic contacts during the initial rearrangement process and throughout the entire test, the TRUBAL is an adequate model. A density scaling method has been used to increase the magnitude of the time step in order to ensure the completion of the simulations within a reasonable period (Sheng et al., 2001).

Table 1 shows the input properties for the DEM simulations at which the dimension of unit cell was deliberately chosen to match the dimension of the square die in the experiments. The limiting contact pressure refers to the pressure below which the interaction behaviour is assumed to be elastic (Thornton and Ning, 1998). The values of limiting contact pressure and internal friction coefficient are various as the degree of particle consolidations differs throughout the compaction processes.

3.2. Finite element method

An axisymmetric model (see Fig. 3) was constructed using a commercial software package ABAQUS 6.1 (Hibbitt et al., 2002) to simulate the current die compaction process. Half of the axial section of the compact, punch and die wall were meshed and axisymmetric boundary conditions were applied at the

Table 1
Properties used in the DEM simulations of the square die compaction tests

Dimension of unit cell	12 mm × 12 mm × 7 mm
Diameter of particles	450–650 μm
Mean diameter of particles	600 μm
Number of particles in a unit cell	3200
Young's modulus of particles	3.5 GPa
Poisson ratio of particles	0.3
Internal friction coefficient	0.3–0.5
Limiting contact pressure	20–200 MPa

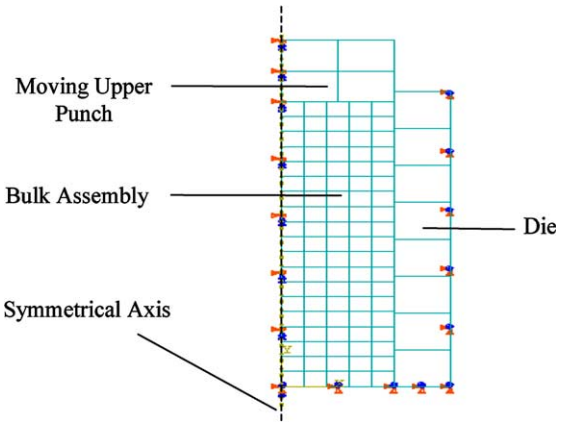

Fig. 3. Axisymmetric mesh used in the FEM simulations of the uniaxial single-sided cylindrical die compaction tests.

Table 2
Material parameters adopted for the implementation of the Drucker–Prager/cap model (Drucker and Prager, 1952)

Young's modulus	9.03 GPa
Poisson ratio	0.28
Internal angle of friction	16.5°
Material cohesion	5.5 MPa
Cap shape parameter	0.558
Transition surface parameter	0.03

central line. The bottom of the powder bed and die wall were all constrained in both the X- and Y-directions. Explicit dynamical steps were created to simulate the whole loading, unloading and ejection procedures. The interfacial stress contact between the powder bed with the upper punch and die wall was assumed to follow a conventional Coulombic slide line model (Coulomb, 1776). The Drucker-Prager/Cap model (Drucker and Prager, 1952) was adopted as the constitutive model to represent the material behaviour during the constrained rigid die compaction process. The material parameters which were adopted are listed in Table 2. The Young's modulus in Table 1. refers to the Young's modulus of agglomerates, which was evaluated from a micro-compression test. The Young's modulus in Table 2. relates to the Young's modulus of the bulk assembly which was determined experimentally (Aydin, 1994). Contours of the computed in situ density distributions at each stage of the compaction including loading, unloading and ejection were obtained by manipulating the logarithmic strain field output in the ABAQUS software.

4. DEM analysis

4.1. Mechanical responses and compaction mechanisms of the bulk assemblies

A series of DEM calculations were incrementally implemented in order to simulate the same conditions as those produced with the experimental arrangement. The values of the various material parameters were adjusted during the loading and unloading processes since their yielding behaviours strongly depended upon the degree of consolidation and in turn the imposed compression pressure.

To interpret the compaction mechanisms, it is sensible to plot a compaction curve, such as is presented in Fig. 4, from the loading data. In this compaction curve, the average density of the bulk assemblies is plotted against the compaction pressure to demonstrate the pressure–volume characterisation. The results from the DEM simulations in Section 3.1 agree remarkably well with the experimental results. It is clearly shown that the loading process can be divided into at least three stages. In stage I, the particles mobilised and rearranged to fill the voids available in the bulk system. Despite the low and uniform load taken by the bulk assemblies, this stage involves particularly complex mechanisms since the axial and lateral movements of the particles are entirely unpredictable.

In stage II, the particles start to compress against each other at the first yielding point, ca. 0.5 MPa in this case, as the compaction pressure is increased. The porosity of the bulk assemblies reduces when the voids are gradually filled. Elastic deformations of the particles are extensive and plastic deformations, at some contacts of particles, also begins. In stage III, most of the particles will have undergone extensive significant plastic deformation and breakdown of the agglomerates into primary particles is observed when the local pressure exceeds the agglomerate strength. A rearrangement of the primary particles may also be involved. In fact, the various stages may overlap due to the natural inhomogeneous stress localisations. The boundary of stages II and III is indistinct and the yielding point in Fig. 4 may only be determined approximately through a microscopic responses analysis, as is explained in Section 4.2. In the final stage, the further densification of the bulk assemblies becomes difficult to achieve even when the compaction pressure is very high. This phenomenon is known as the strain hardening phase of the bulk assemblies.

4.2. Microscopic responses of the alumina agglomerates

Apart from the macroscopic characterisation, the DEM results are also able to demonstrate the microscopic likely behaviour of the compressed particles during the compaction processes (Sheng et al., 2001). Fig. 5(a) and (b) illustrate the evolution of the inter-agglomerate particle compact coordination number and also the plastic contact number of the particles with respect to the extent of the imposed nominal axial strain. The plastic contact number, of a particulate assembly, is defined as the number of the inter-particle contacts that have exceeded the assumed inter-particle elastic yield stress. The average coordination number increases with the increasing of the compaction load and the rate of this increase is dependent upon the response during the different compaction stages, as is shown in Fig. 4. In the particle rearrangement stage, many particles are easily free to move, few contacts may be set up and, therefore, the coordination number is low and also slowly varying. When all of the available voids are "filled-up" with

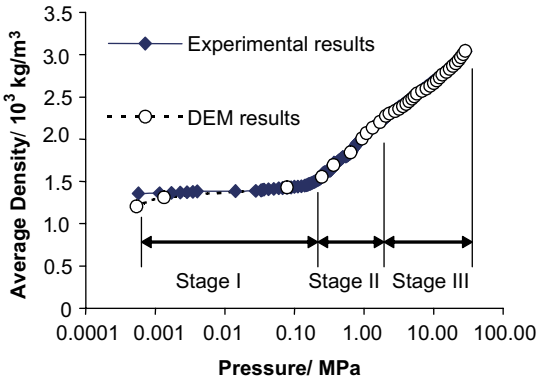

Fig. 4. Compaction curves of the square die compaction tests.

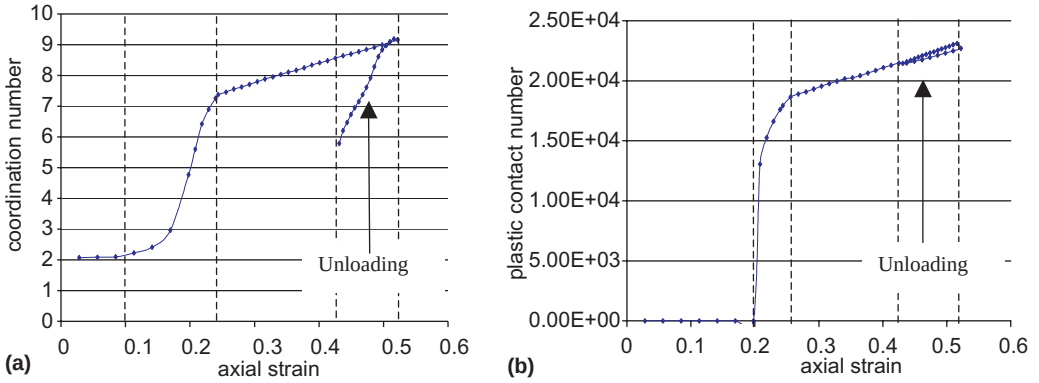

Fig. 5. Evolution of the (a) the computed coordination number and (b) its computed plastic contact number in square die compaction tests.

particles, which occur, in this case, at an axial strain of ca. 0.1, the particle contacts begin to "lock-up" and the coordination number then increases sharply. The initial contacts are primarily elastic until the localised stress exceeds the yield stress of the particles at an axial strain of ca. 0.2.

Following the rearrangement of the particles and extensive plastic deformations at the contacts, the coordination number undergoes a steady increase with the increasing of the imposed axial strain. When the compaction load is removed, the contacting particles partially recover their original shape and recoil by relaxing the elastic strain energy stored during the loading process. Hence, the coordination number decreases significantly as some, a small faction, of the imposed particle contacts are broken. Since, at this stage, almost all of the particles were plastically deformed, the plastic contact number only decreases by a small amount.

5. FEM analysis

5.1. Evolution of stress localisation and structural inhomogeneity

A quantitative prediction of the in situ stress and density distributions using the FEM modelling are shown in Figs. 6–12. It should be noted that original Figs. 9–12 are in red green blue (RGB) primary colours while they are presented here in greyscale. Figs. 6–8 depict the density contours predicted under the different deformation conditions. The axis of symmetric is on the left side and the moving punch loads at the top. The upper circumference zone of the green compact was found to coincide with the region of highest local density whereas the lowest density region was found to lie at the bottom circumference. These findings are in agreement with the results previously obtained and reported in the literature (Ozkan, 1994; Aydin, 1994). The structural variation is primarily caused by the friction work between the die wall and the adjacent particles, with inter-particle friction providing a minor contribution.

The above-mentioned phenomenon is consistent with the stress contours obtained from the FEM results, as are illustrated in Figs. 9–11. In Figs. 9–11, the regions with darkest colour refer to the densest and loosest states, which are designated as T and B respectively. Both the axial and radial stress contours at the maximum load show a significant difference in their magnitudes between the stresses at the top (T) and bottom (B) corners. The particles in the region near the top corner sustained a larger localisation stress and conversely the particles in the region near the bottom corner were preserved from being intensely deformed.

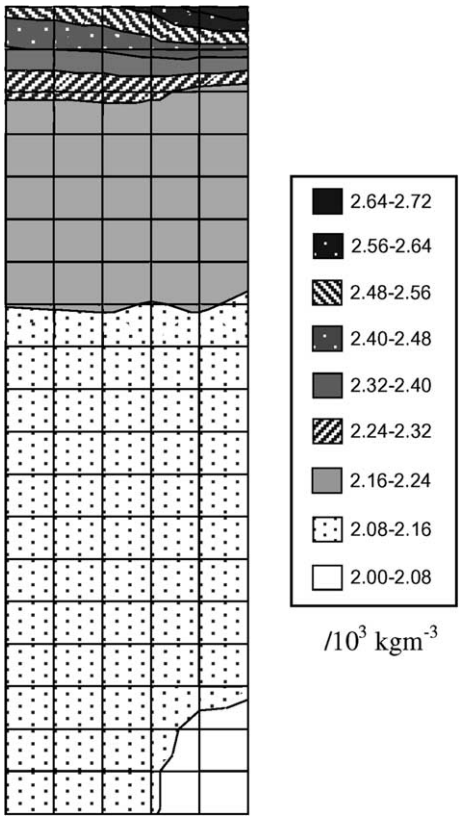

Fig. 6. Density contours at maximum loading (91.3 MPa) from the FEM results.

Fig. 12 shows the radial stress contours of the green compact during the ejection process. The bottom section of the green compact that was extruded from the die comprised a more uniform stress distribution. This section also underwent a stress relaxation while the remaining section was still under stress condition. The development of a series of cracks is possible if the imposed stress exceeds the material ultimate shear fracture strength.

5.2. Stress localisation during the loading process

Fig. 13 schematically illustrates the generation of the local forces present within a uniaxial single-ended die-pressed green compact (Train, 1956). When a force is applied, at equilibrium, the upward (u) and downward (d) components of the axial force at the upper corner are resisted by the upper punch and the lower layers of particles. Meanwhile, the outward (o) and inward (i) components of the radial force are balanced by the die wall and particles at the centre. As a result, a resultant force (r) resembling a conical surface with a focus point is created. Due to the symmetry of the system, the conical forces combine and give rise to a net resultant force (r_c), which are responsible for the high-density region at the bottom centre. The particles in region A experience neither a severe shearing force nor an axial force, leading to a low degree of deformation and low-density region. Similarly, the particles in region B, adjacent to the static bottom punch do not move appreciably. Therefore, the shearing force is negligible and the density in this region is also relatively low.

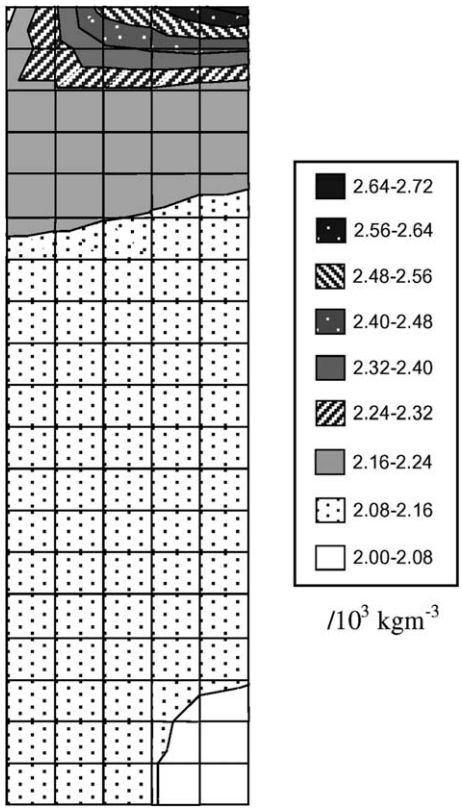

Fig. 7. Density contours after unloading from the FEM results.

Fig. 14 shows the Train result from a series of compaction experiments for magnesium carbonate powders. The local densities were represented by % solid. By comparing Figs. 6–8 to Fig. 14, both of the results show a very similar density distribution contour. A high density region was found to coincide with the top circumference of the compact whereas the bottom circumference was found to have the lowest density. Figs. 6–8, however, show a more intense density at the top circumference whereas the Train results indicate a more uniform density distribution throughout the compact due to the application of lubrication on the die wall. This comparison clearly demonstrates that wall friction is a main controlling factor in compaction processes.

5.3. Attenuation of the stress transmission during the compaction processes

As well as illustrating the evolution of the structural inhomogeneity, the FEM results also quantify the stress transmission attenuation during the compaction processes. The green compacts were divided into slabs with a low aspect ratio from the bottom to the top. The average densities of the slabs were evaluated at the maximum load, as well as after unloading and ejection. A curve of average slab density against the distance from the bottom surface is shown in Fig. 15. Inspection of this figure reveals that the slab density increases as the distance from the bottom surface increases in all stages of compaction processes. As was mentioned earlier, the frictional force at the die wall resists the downwards particle movements induced by the applied force during the loading process. The slab at the top of the green compact exhibits the highest

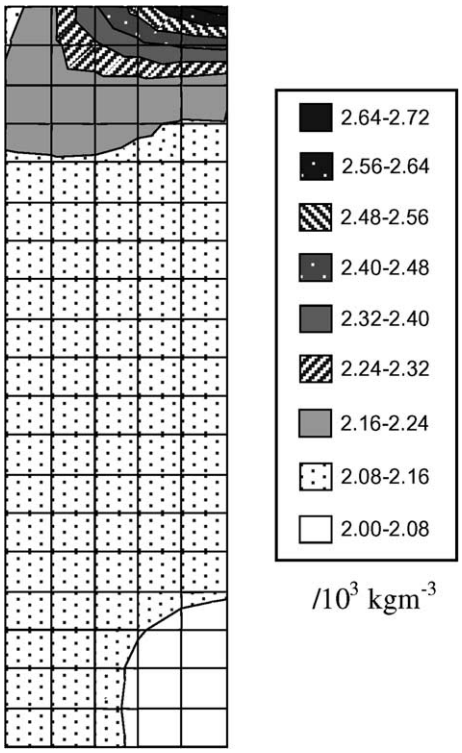

Fig. 8. Density contours after ejection obtained from the FEM results.

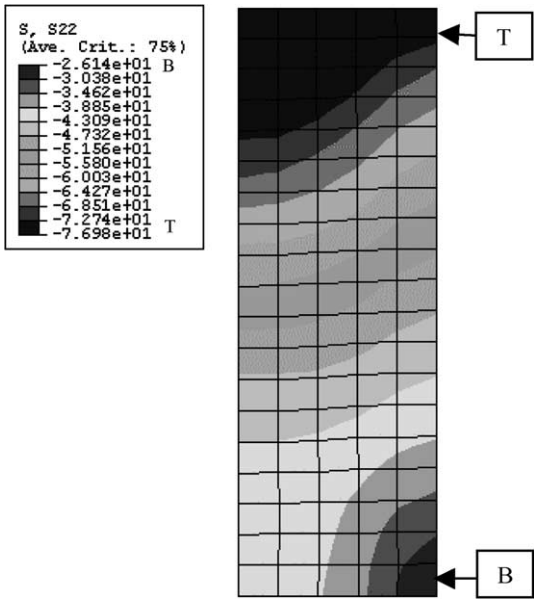

Fig. 9. Axial stress contours at maximum loading obtained from the FEM results.

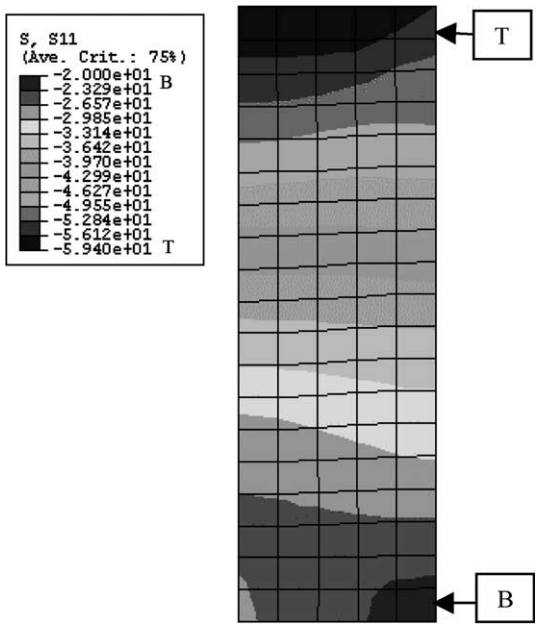

Fig. 10. Radial stress contours at maximum loading obtained from the FEM results.

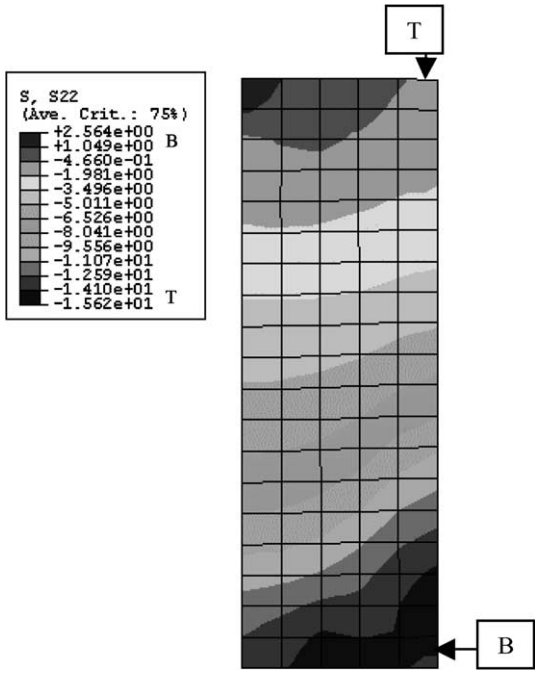

Fig. 11. Axial stress contours following unloading obtained from the FEM results.

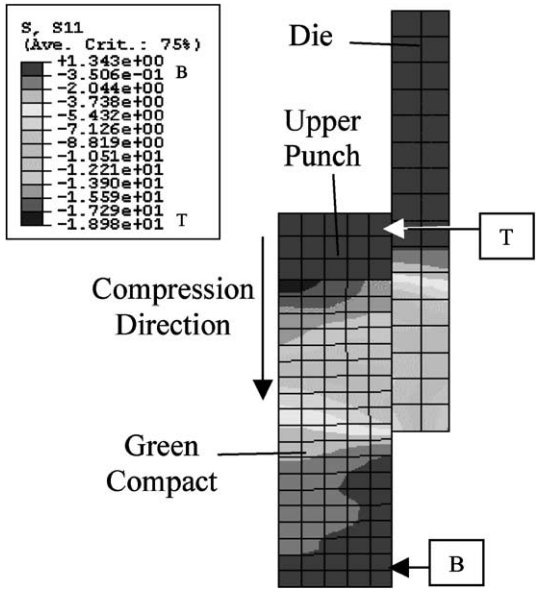

Fig. 12. Radial stress contours during ejection obtained from the FEM results.

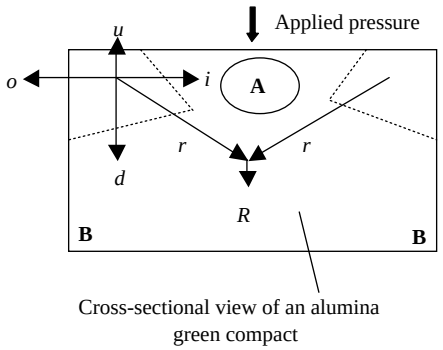

Notation	Description
A	Upper centre
B	Bottom corners
u	Upward force
d	Downward force
i	Inward force
o	Outward force
r	Resultant force
R	Net resultant force

Fig. 13. Illustration of the local forces present within a green compact (Train, 1956).

density, indicating a more intense stress localisation and a higher degree of deformation in that region. The slab density decreases steadily when it approaches the bottom of the compact. This part of result shares the similarity with the predictions of the Janssen–Walker Model (Janssen, 1895; Walker, 1966) which elucidates the variation of the stress transmission attenuation from the pressure source.

6. Morphological analysis

Fig. 16 shows SEM images taken from the diametric fractured cross-section of the alumina green compacts pressed at 20 and 100 MPa respectively. The inter-agglomerates boundaries are very clearly discernible for the low-density regions. The agglomerates are still 'intact' within the low-density region

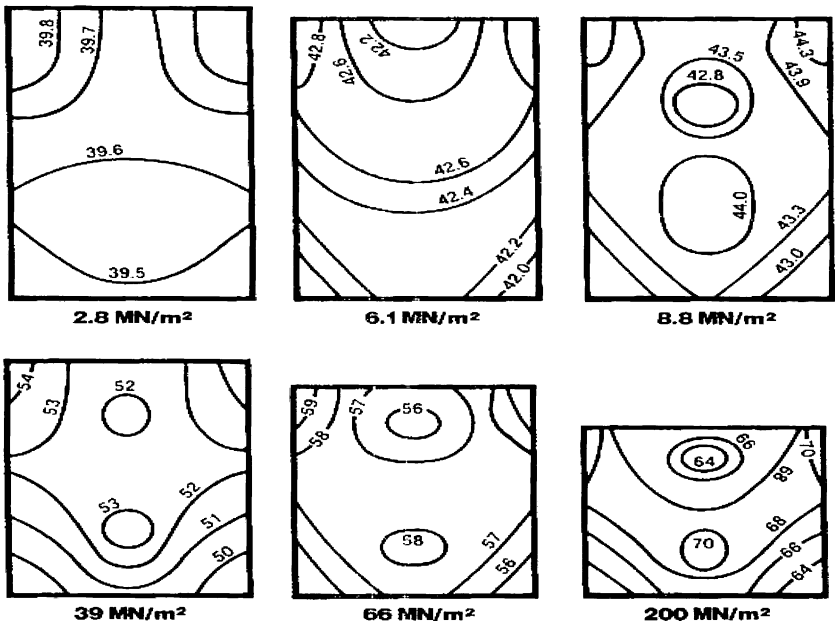

Fig. 14. % Solid distributions in lubricated die-pressed compacts of magnesium carbonate powders at various pressures (Train, 1957).

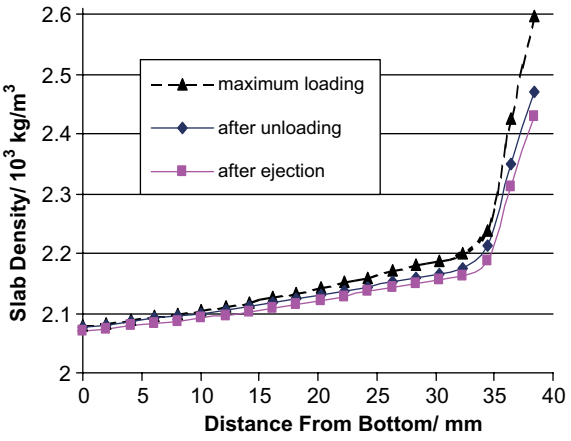

Fig. 15. Variation of the average density of slabs with distance from the bottom of the compact at maximum loading (91.3 MPa).

whereas for the high-density region, particularly the compact pressed at 100 MPa [Fig. 16(c)], the inter-agglomerates boundaries are now largely absent. This suggests that the agglomerates were crushed to their primary particles at the mentioned pressure. By comparing the high-density regions, between the compacts pressed at 20 and 100 MPa [Fig. 16(b) and (c)], the former still partially exhibits some inter-particle boundaries whereas the latter shows no trace of these boundaries, indicating that the top circumference at the compact pressed at 100 MPa experiences an almost total elimination of the internal pores. Fig. 17 summarizes the general distribution of the relatively high and low-density regions.

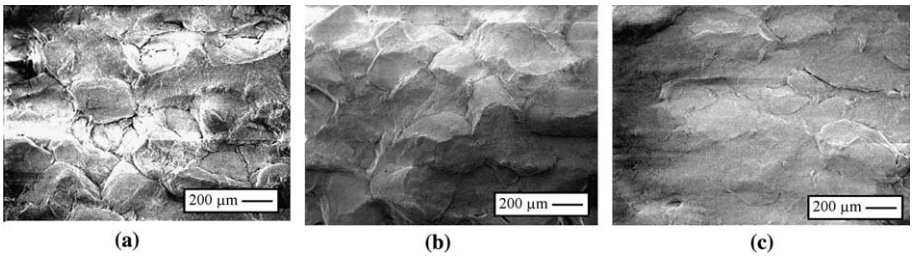

Fig. 16. (a) Bottom corner (low-density region), (b) top corner (high-density region), (c) top corner (high-density region) SEM images of the cross-sections of green compact die-pressed at [(a) and (b)] 20 and (c) 100 MPa.

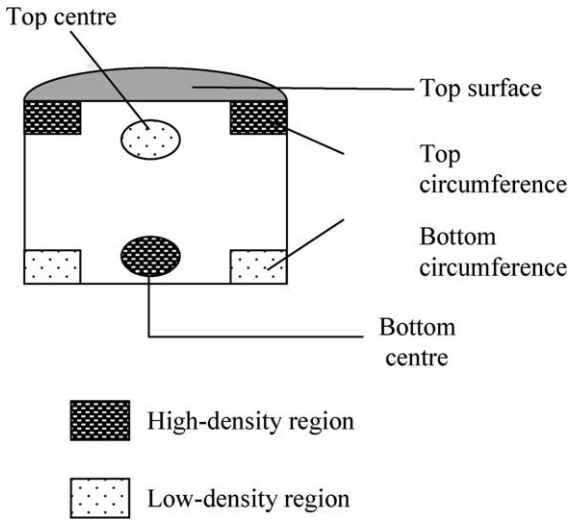

Fig. 17. Cross-sectional view of an alumina green compact indicating the variations in density.

7. Conclusion

At least three distinct stages were distinguished in the compaction processes, namely particle rearrangement; breakdown of agglomerates, elastic and plastic deformation; and strain hardening of bulk assemblies. A comparison of the experimental and the DEM results has demonstrated the potential of the DEM simulations to rationalise the mechanical responses of particles at microscopic level during the compaction processes. From the FEM results and the SEM image analyses, the top circumference is classified as the highest local density and vice versa. This structural inhomogeneity is primarily caused by the inter-particle frictional work and frictional work between the die wall and the adjacent particles.

Acknowledgements

The research work of this study is supported by Engineering and Physical Sciences Research Council (Grant GR/N13050) in United Kingdom. Special thanks to Dr. Colin Thornton from University of Birmingham for providing us the DEM TRUBAL code.

References

Aydin, I., 1994. Near-net-shape Forming of Ceramic, Ph.D. Thesis, Imperial College London.
Aydin, I., Briscoe, B.J., Sanliturk, K.Y., 1996. The internal form of compacted ceramic components: a comparison of a finite element modelling with experiment. Powder Technology 89, 239–254.
Briscoe, B.J., Sinha, S.K., 1997. Density distributions characteristics of green ceramic compacts using scratch hardness. Tribology International 30, 475–482.
Cooper Jr., A.R., Goodnow, W.H., 1962. Density distribution in dry pressed compacts of ceramic powders examined by radiography of lead grids. Bulletin American Ceramic Society 41 (11), 760–761.
Cundall, P.A., Strack, O.D.L., 1979. A discrete numerical model for granular assemblies. Geotechnique 29, 47–65.
Drucker, D.C., Prager, W., 1952. Soil mechanics and plastic analysis of limit design. Quarterly of Applied Mathematics 10, 157–175.
Hibbitt, Karlsson, Sorensen, 2002. ABAQUS/ Explicit User's Manual Version 6.3.
Ozkan, N., 1994. Compaction and sintering of ceramic powders, Ph.D. Thesis, Imperial College London.
Oda, M., Iwashita, K., 1999. Mechanics of Granular Materials: An Introduction. A.A. Balkema Publishers, Rotterdam, Netherlands.
Sheng, Y., Briscoe, B., Aydin, I., Lawrence, C., 2001. An explanation of internal density gradients during the entire compaction cycle of powders. Proceedings of Fine Powder Processing 2001, 207–213.
Thornton, C., Ning, Z., 1998. A theoretical model for the stick/bounce behaviour of adhesive, elastic–plastic spheres. Powder Technology 99, 154–162.
Thornton, C., Sun, G., 1993. Uniaxial compression of granular media: numerical simulation and physical experiment. Powders and Grains 93, 129–134.
Thornton, C., Yin, K., 1991. Impact of elastic spheres with and without adhesion. Powder Technology 65, 153–166.
Train, D., 1956. An investigation into the compaction of powders. Journal Pharmacy and Pharmacology 8, 745–761.
Train, D., 1957. Transmission of forces through a powder mass during the process of pelleting. Transactions Institution Chemical Engineers 35, 258–266.
Walker, D.M., 1966. An approximate theory for pressures and arching in hopper. Chemical Engineering Science 21, 975–997.